Structural Characteristics of Cerium Oxide Nanocrystals Prepared by the Microemulsion Method

J. Zhang,* X. Ju, Z. Y. Wu, T. Liu, T. D. Hu, and Y. N. Xie

Beijing Synchrotron Radiation Facility, Institute of High Energy Physics, Chinese Academy of Sciences, Beijing 100039, P. R. China

Z. L. Zhang

Beijing Laboratory of Electron Microscopy, Institute of Physics and Center for Condensed Matter of Physics, Chinese Academy of Sciences, Beijing, 100080, P. R. China

Received March 20, 2001. Revised Manuscript Received August 8, 2001

The aim of this work is to investigate the microstructure development of cerium oxide nanocrystal, prepared by the microemulsion process, as a function of annealing temperature in air. Combined with the HRTEM and the thermogravimetric−differential thermal analysis (TG−DTA), the XRD patterns reveal that the sample annealed at 623 K is amorphous, and the formation of cerium oxide nanocrystal occurs above 773 K. The local structural and electronic properties in the nanocrystallization process are probed by X-ray absorption spectra (XAS) at the Ce L_3 edge. It is found that the phase structure changes from triclinic to cubic (CeO_2), and the electronic structure changes from Ce^{3+} to Ce^{4+} upon increasing the annealing temperature.

1. Introduction

Nanocrystal rare earth oxides, RO_x, where R ≃ Ce, Pr, Tb, etc., are playing an increasingly important role in solid-state physics, chemistry, and materials science.[1−8] By precisely controlling the size and surface properties of these nanocrystals, their chemical and physical properties can be manipulated.[4−6] The ability to make nanocrystals of high quality and to understand the microstructure properties in the nanocrystalline process is key to this area of science.

The development of the microemulsion method offers a good way to obtain the nanocrystals with controlled surface and size;[6,9] usually, the preparation of RO_x nanocrystal in the microemulsion process involves two steps. One is to prepare rare earth oxide nanoparticles in a water-in-oil (w/o) microemulsion, which is a transparent, isotropic liquid medium with nanosized water droplets dispersed in a continuous oil phase and stabilized by surfactant molecules at the water/oil interface. These surfactant-covered water pools offer a unique microenvironment for the formation of nanoparticles. They act as microreactors for processing reactions and inhibit the excess aggregation of particles. As a result, the particles obtained in such a microenvironment are generally very fine and monodispersed.[10−12] The other step in the process is to crystallize the nanoparticles by increasing the annealing temperature. The properties of nanocrystal, such as crystalline size, shape, strain, and stacking faults, are governed by the chemical nature of the "microreactor" and the annealing process of the nanoparticles. To obtain nanocrystals with controlled properties, it is necessary to investigate the structural characteristics of the nanocrystal during its formation and growth.

Generally, varied techniques are used to characterize the nanocrystalline process, such as electron microscopy, gas absorption, and X-ray diffraction line broadening analysis. They yield much information about the shape of the nanocrystal and the long-range order of the atoms.[13−15] However, local structure and electronic properties, which determine the essential properties of the materials, are still unknown. X-ray absorption spectroscopy (XAS), including X-ray absorption near edge structure (XANES) and extended X-ray absorption fine structure (EXAFS), as a unique element-specific technique sensitive to the local structure, can provide insight into local environment as well as electronic structures of materials. In particular, XANES studies

* Corresponding author. Telephone: 8610-68235980. Fax: 8610-68275347. E-mail: jzhang@ihep.ac.cn.

(1) Zarur, A. J.; Ying, J. Y. *Nature* **2000**, *403*, 65.
(2) Luca, V.; Djajanti, S.;Howe, R. F. *J. Phys. Chem. B* **1998**, *102*, 10650.
(3) Chen, L. X.; Rajh, T.; Wang, Z.; Thurnauer , M. C. *J. Phys. Chem. B* **1997**, *101*, 10688.
(4) Chen, S.; Ida, T.; Kimura, K. *J. Phys. Chem. B* **1998**, *102*, 6169.
(5) Tsunekawa, S.; Fukuda, T.; Kasuya, A. *J. Appl. Phys.* **2000**, *87*(3), 1318.
(6) Tsunekawa, S.; Sivamohan, R.; Ohsuna, T.; Kasuya, A. *Mater. Sci. Forum*. **1999**, *315−317*, 439
(7) Nitsche, R.; Winterer, M.; Croft, M.; Hahn, H. *Nucl. Instr. Methods B* **1995**, *97*, 127.
(8) Ying, J. Y.; Tschope, A. *Chem. Eng. J.* **1996**, *64*, 225.
(9) Milan-Johann, S.; Katrin, S. *Chem. Rev.* **1995**, *95*, 849.
(10) Luisi, P. L.; Magid, L. J. *CRC Crit. Rev. Biochem*. **1986**, *20*, 409.
(11) Pileni, M. P., Ed. *Structure and Reactivity in Reverse Micelles*; Elsevier: Amsterdam, 1989.
(12) Paul. B. K.; Moulik, S. P. *J. Dispersion Sci. Technol.* **1997**, *18*, 301. (b) Dong, H. C.; Szu, H. W. *Chem. Mater.* **2000**, *12*, 1354.
(13) Yu, X. H.; Li, F.; Ye, X. R.; Xin, X. Q.; Xue, Z. L. *J. Am. Cerm. Soc.* **2000**, *83*(4), 964.
(14) Audebrand, N.; Louer, D. *J. Phys. IV, Proc. (Fr.)* **1998,** *8*(5), 109.
(15) Guillou, N.; Nistor, L. C.; Fuess, H.; Hahn, H. *Mater. Sci. Forum* **1998**, *278−281*(2), 879.

10.1021/cm010235p CCC: $20.00
Published on Web 10/11/2001

Table 1. Peak Positions and Assignments in the Ce L_3-edge XANES Spectra of Selected Samples[a]

sample	peak A, 5717.8 eV	peak B, 5724.6 eV	peak C, 5725.5 eV	peak D, 5728.2 eV	peak E, 5735.3 eV
1. $Ce(NO_3)_3{\cdot}6(H_2O)$			$2p \rightarrow 4f^L5d$		
2. as-prepared			$2p \rightarrow 4f^L5d$		
3. nano-CeO_{2-x}-473 K			$2p \rightarrow 4f^L5d$		
4. nano-CeO_{2-x}-623 K			$2p \rightarrow 4f^L5d$	$2p \rightarrow 4f^L5dt_{2g}L$	$2p \rightarrow 4f^L5d$
5. nano-CeO_2-773 K	$2p \rightarrow 5d$	$2p \rightarrow 4f^L5dt_{2g}L$		$2p \rightarrow 4f^L5dt_{2g}L$	$2p \rightarrow 4f^L5d$
6. nano-CeO_2-873 K	$2p \rightarrow 5d$	$2p \rightarrow 4f^L5dt_{2g}L$		$2p \rightarrow 4f^L5dt_{2g}L$	$2p \rightarrow 4f^L5d$
7. bulk CeO_2	$2p \rightarrow 5d$	$2p \rightarrow 4f^L5dt_{2g}L$		$2p \rightarrow 4f^L5dt_{2g}L$	$2p \rightarrow 4f^L5d$

[a] L denotes an oxygen ligand 2p hole.

at L_3 thresholds of the rare-earth (RE) play an essential role due to their simplicity and universal applicability.[16−18] Therefore, it is amendable to the XRD and TEM. In this paper, TG−DTA, XRD, HRTEM, and XAS are used to investigate the microstructure development of the nanocrystal cerium oxide, prepared by the microemulsion process, which will give a guide for the design and preparation of new nanocrystals.

2. Experimental Section

Preparation of the CeO_{2-x} Microemulsion: The cationic surfactant cetyltrimethylammonium bromide (CTAB, 5 g) was dissolved in 200 mL of cyclohexane and 8 mL of butanol. This solution was stirred for 20 min and became transparent. Then 2 mL of 0.5 M $Ce(NO_3)_3{\cdot}6H_2O$ and 2 mL of 10% $NH_3{\cdot}H_2O$ was added to the solution with vigorous stirring, respectively. After that, the two resulting solutions were mixed and formed a transparent CeO_{2-x} microemulsion.[19]

The nanometer CeO_{2-x} ($0 < x < 2$) powder was obtained from the microemulsion by rotary evaporatation and then was heat-treated at 473, 623, 773, and 873 K for 2 h in air. The resulted samples are labeled as as-prepared (sample 2), nano-CeO_{2-x}-473 K (sample 3), nano-CeO_{2-x}-623 K (sample 4), nano-CeO_2-773 K (sample 5), and nano-CeO_2-873 K (sample 6), as shown in Table 1.

TG−DTA thermal analysis employed a SDT 2960 simultaneous TGA−DTA instrument. The temperature range for scanning was from 20 to 900 °C and the scanning speed was 10 °C/min.

The X-ray diffraction (XRD) patterns for all the samples were recorded on a Rigaku D/max-IIB type Cu−K XRD. The particle size of CeO_2 was calculated from the Scherrer formula using the (220) diffraction peak of respective cerium oxide.[20]

The high-resolution transmission electron microscopic (HRTEM) measurements were carried out using a Hitachi H-7100 electron microscope operating at 200 kV. The samples for the HRTEM measurements were dispersed in alcohol before being transferred to the carbon-coated copper grids.

XAS spectra at the Ce L_3 edge were measured in transmission mode by using synchrotron radiation with a Si(111) double crystal monochromater at the EXAFS station (Beam line 4W1B) of Beijing Synchrotron Radiation Facility. The storage ring was run at a typical energy of 2.2 GeV with the electron current about 80 mA. To suppress the unwanted harmonics, the angle between the monochromater crystal faces was adjusted to mistune the incident beam by 30%. The incident and output beam intensities were monitored and recorded using a nitrogen gas and a 50% argon-doped nitrogen flowing ionization chamber. The spectra were scanned in the range of 5.5−6.2 keV, which covers the L_3 edge absorption of cerium atoms. Energy resolution was about 1.5 eV for XANES and about 3.0 eV for the EXAFS.

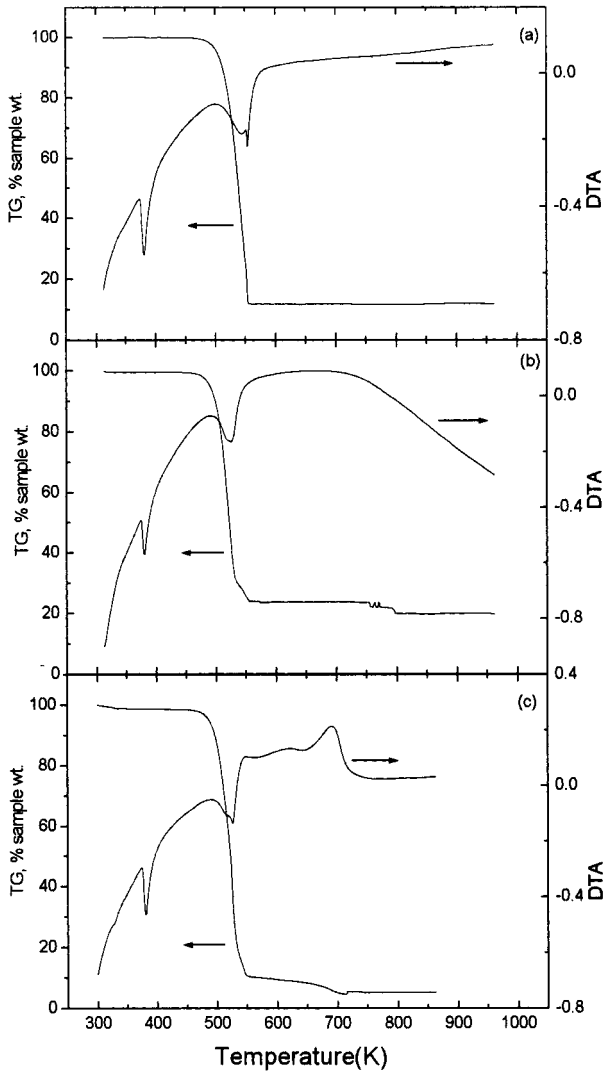

Figure 1. TG−DTA curves of CTAB in nitrogen (a) and the as-prepared sample in nitrogen (b) and air (c), respectively.

The EXCURV92 program (Daresbury) was used for data analysis. The midpoint of the absorption jump was chosen as the energy threshold (5723 eV). The preedge absorption background was fitted and subtracted by using the Victoreen formula. The postedge absorption backgrounds were fitted by using the spline function and subtracted from the absorption spectra. The EXAFS functions were normalized by using the absorption edge jump and were Fourier transformed to *R*-space with k^3-weighing over the range from 3.3 to 9.5 Å. Phase shift was corrected using theoretical calculations.

3. Results

3.1. TG−DTA. Figure 1 shows the thermal-analysis spectra of CTAB in nitrogen (a), as-prepared sample in

(16) Borgna, A.; Stagg, S. M.; Resasco, D. E. *J. Phys. Chem. B,* **1998**, *102*, 5077.
(17) Chang, C. L.; Dong, C. L.; Huang, C. L. *J. Appl. Phys.* **2000**, *87*(7), 3349.
(18) Nachimuthu, P.; Wen, C. S.; Ru, S. L.; Ling, Y. J.; Jin, M. C. *J. Solid State Chem.* **2000**, *149*, 408.
(19) Bin, W. Z.; Ping , W. L.; Yan, H. G. *Chin. J. Appl. Chem.* **1999**, *16*(6), 9.
(20) Audebrand, N.; Auffredic, J. P.; Louer, D. *Chem. Mater.* **2000**, *12*, 1791.

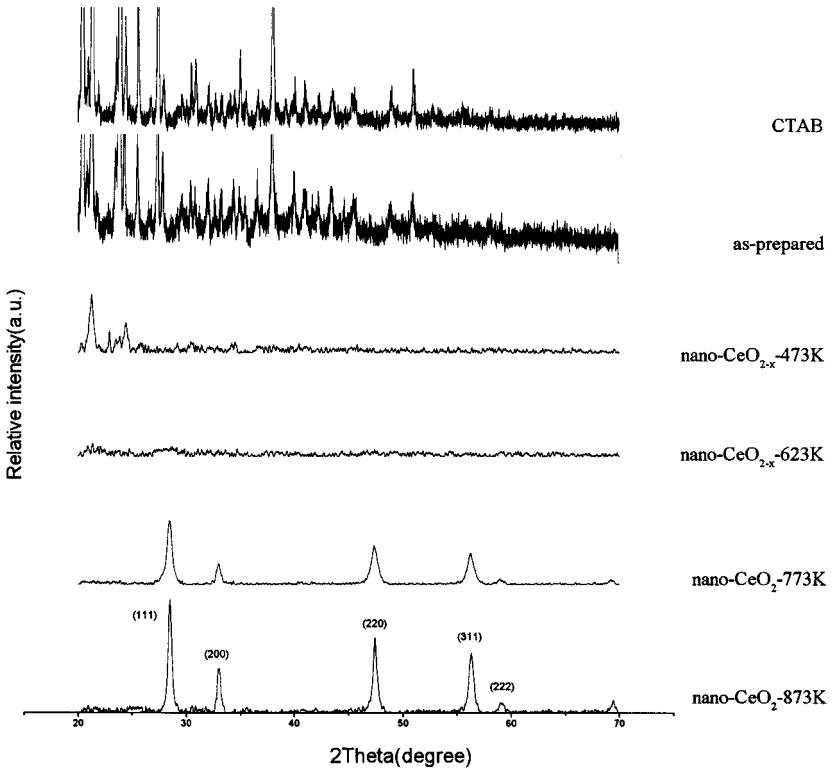

Figure 2. XRD patterns of selected samples.

nitrogen (b) and air (c), respectively. It is observed in all curves that there is an endothermic peak around 380 K corresponding to the melting of the CTAB. For the CTAB under N_2 atmosphere in Figure 1a, the endothermic peak at 551 K with the total rate of weight loss about 89% resulted from the decomposition and endothermic reaction of CTAB.[19] For the as-prepared sample, which involves CTAB and Ce compound, the thermal behavior under N_2 atmosphere can be observed in Figure 1b. It is shown that the decomposition temperature of CTAB is down to 525 K, with a weight loss of 76%. This may result from the Ce compound interacting with CTAB. In this decomposition process, CTAB is changed into some organic species (A). The relatively wider peak in the range of 527−777 K, with a weight loss of 5%, is caused by the decomposition of organic species A and Ce compound. For the as-prepared sample under air atmosphere in Figure 1c, the decomposition temperature of the CTAB is 523 K, with a weight loss of 90% mainly attributed to the decomposition and oxidation of CTAB. In this process, CTAB is changed into some organic species (B), which can further oxide in the range of 563−623 K. Moreover, the exothermic peak emerged around 692 K, with a weight loss of 4%, which was caused by the oxidation of Ce compound and formation of CeO_2. This can be confirmed by the XRD results given in Figure 2, where the CTAB is completely removed from the as-prepared sample and CeO_2 phase is formed above 623 K.

3.2. XRD. The XRD patterns of selected samples are shown in Figure 2. For the as-prepared sample, the features in the XRD pattern are consistent with that of the CTAB. When the annealing temperature increases but is still below 623 K, the intensities of the diffraction peaks of CTAB gradually decrease. For the sample annealed at 623 K, the diffraction peaks of CTAB disappear, and the amorphous feature emerged. Upon further increasing the annealing temperature to 773 K, all the reflections of cerium(IV) oxide, which is corresponding to the cubic fluorite structure with space group $Fm3m$ and lattice constant $a = 5.4$ Å, are observed. After applying the Scherrer formula to the (220) diffraction peak of cerium oxide,[20] the crystallite size of cerium oxide nanoparticles are 4 nm at 773 K and 7 nm at 873 K, respectively.

3.3. HRTEM. The HRTEM pictures of as-prepared sample annealed at different temperature are shown in Figure 3. When the annealing temperature is 623 K, it is observed that there are many aggregates that are of spherical shape with a size of about 65 nm. In addition, there are some clusters having a spherical particle, which is amorphous from the electron diffraction (ED) pattern. On the other hand, the cerium oxide nanocrystal with a diameter of 6−8 nm appears when the annealing temperature increases up to 873 K. From the ED pattern, the nanocrystal can be assigned to be the cubic phase of CeO_2. Obviously, this observation is consistent with the result of XRD and supports the formation of the cerium oxide nanocrystal.

3.4. XANES. To better elucidate the structural and electronic nature of the Ce site in the investigated system, we have performed Ce L_3-edge XANES measurements. For comparison purposes, we have also obtained Ce L_3-edge XANES spectra of reference compounds such as $Ce(NO_3)_3 \cdot 6H_2O$ with triclinic structure and CeO_2 in the cubic phase. Figure 4 compares the normalized Ce L_3-edge XANES spectra of select samples. The assignments of Ce L_3-edge spectra, based on refs 21−24, are list in Table 1. For the Ce L_3-edge spectrum

(21) Kaindl, G.; Schmiester, G.; Sampathkumaran, E. V. *Phys. Rev. B* **1988**, *38*, 10174.

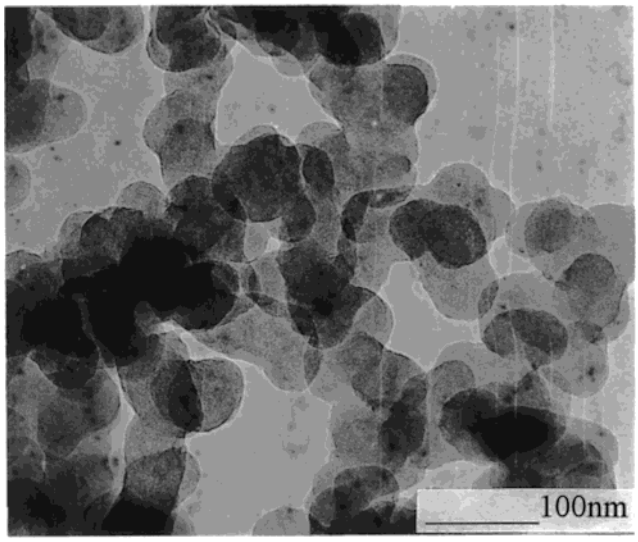

3a

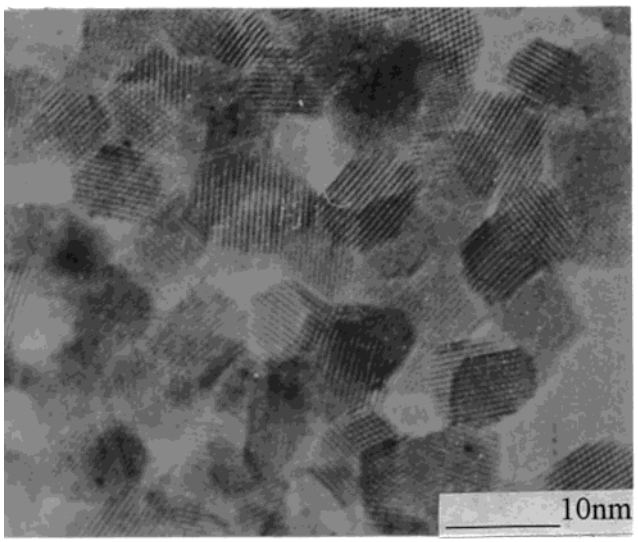

3b

Figure 3. HRTEM of as-prepared sample annealed at 623 K (a) and 873 K (b), respectively.

of standard $Ce(NO_3)_3 \cdot 6H_2O$, the strongest peak C at about 5725.5 eV, due to the dipole-allowed transition of Ce 2p to Ce $4f^15d$ final states, characterizes the Ce in the trivalent state.[24] However, the standard CeO_2 XANES spectrum from 5710 to 5750 eV contains four peaks (A, B, D, E). The preedge structure, labeled A, is assigned to final states with delocalized d character at the bottom of the conduction band. Due to the cubic crystal-field splitting of Ce 5d states, features B and D are associated with the transitions of Ce 2p to the Ce $4f^15d\ e_g$ L and Ce $4f^15d\ t_{2g}$ L states, where L denotes an oxygen ligand 2p hole and $4f^1$ refers to an electron going from an oxygen 2p orbital to a cerium 4f one (charge-transfer-like). The energy separation between peak B and D is about 3.6 eV, which is in agreement

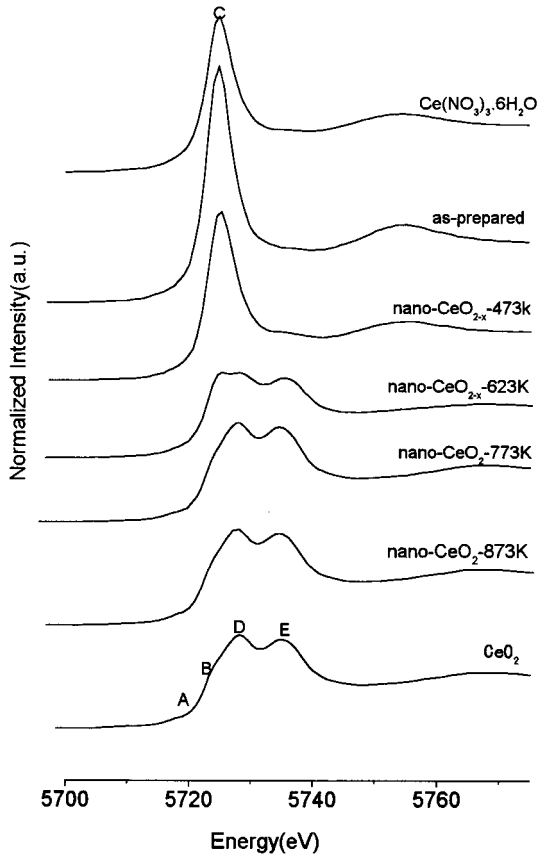

Figure 4. The normalized XANES spectra of selected samples in the range 5700−5775 eV.

with previous works.[22] The feature E is attributed to the contribution of a different final state configuration $4f^05d$. Generally, the Ce spectrum has a distinct double-peaked structure (D, E) with the higher lying peak corresponding to the Ce^{4+} valence state.[24]

For the as-prepared sample and the sample annealed below 473 K, the XANES spectra at Ce L_3 edge has a single peak at about 5725.5 eV, similar to that of crystalline sample $Ce(NO_3)_3 \cdot 6H_2O$ and different from the spectrum of standard CeO_2. As the annealing temperature increases up to 623 K, the spectra show three features (C, D, and E): C is due to Ce^{3+}, while D and E are features of Ce^{4+}. This shows that Ce^{3+} and Ce^{4+} coexist in the CeO_{2-x} nanoparticles when the annealing temperature is in the range between 473 and 623 K. When the temperature is up to 773 K, four different features, labeled A, B, D, and E, are present, which are characteristic features of CeO_2 in the cubic phase.[22]

3.5. EXAFS. EXAFS is employed to examine the surrounding of the Ce in the CeO_{2-x} nanoparticles. Figure 5 shows the observed and best-fit calculated EXAFS and magnitude Fourier transforms for the selected samples. The best-fit parameters for these samples are list in Table 2. From crystallographic data,[25] the EXAFS for the $Ce(NO_3)_3.6(H_2O)$ standard could be fitted with two subshells at 2.64 Å (Ce−O) and 3.26 Å (Ce−N), the corresponding coordination numbers being 11.0 and 3.0, respectively. However, for the CeO_2 standard, the first peak could be fitted with a single shell at 2.34 Å (Ce−O), and coordination number is close to eight.

(22) Soldatov, A. V.; Ivanchenko, T. S.; Longa, S. D.; Kotani, A.; Iwamoto, Y.; Bianconi, A. *Phys. Rev. B* **1994**, *50*, 5074.
(23) Douillard, L.; Gautier, M.; Thromat, N.; Duraud, J. P. *Nucl. Instr. Methods Phys. Res. B* **1995**, *97*, 133.
(24) Capehart, T. W.; Mishra, R. K.; Herbst, J. F. *J. Appl. Phys.* **1992**, *72*(2), 676.
(25) Milinski, N.; Ribar, B.; Sataric, M. *Cryst. Struct. Commun.* **1980**, *9*, 473.

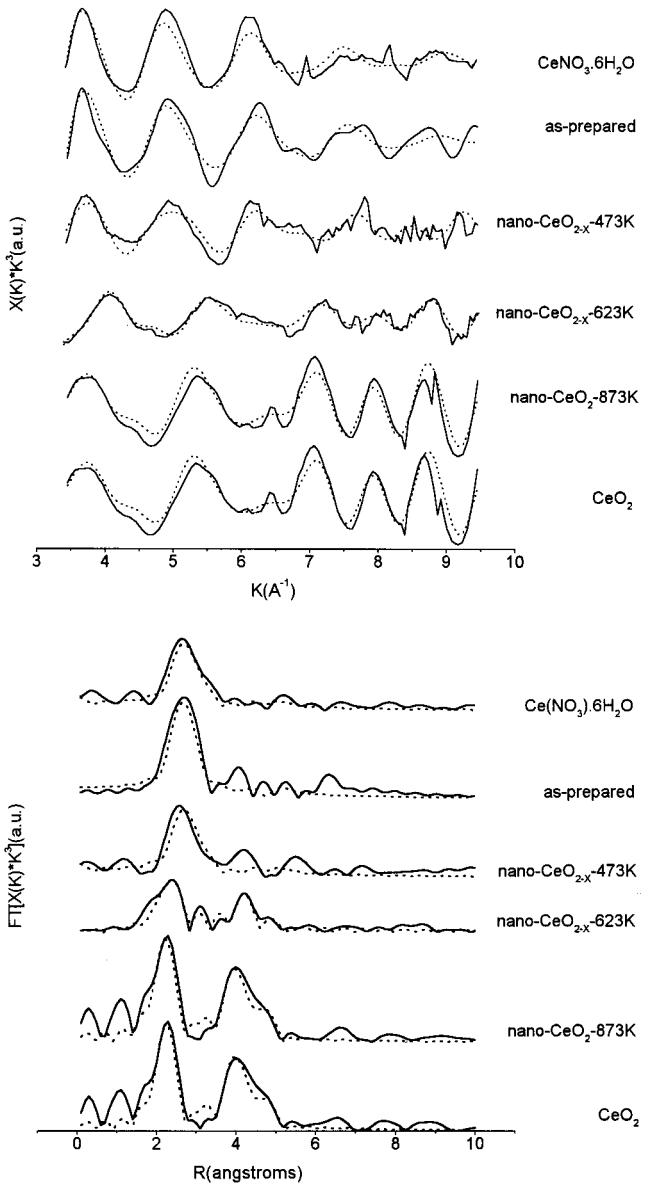

Figure 5. Fitted k^3-weighted Ce L_3-edge EXAFS (a) and the corresponding fitted magnitude FT spectra (b) of selected samples.

Table 2. EXAFS Fit Results for Selected Samples

sample	shell	*N* (±0.5)	*R* (Å) (±0.01)	σ^2 (Å) (±0.001)
$Ce(NO_3)_3{\cdot}6H_2O$	O	11.0	2.64	0.020
	N	3.0	3.26	0.010
as-prepared	O	6.3	2.64	0.001
	O	6.2	2.47	0.006
nano-CeO_{2-x}-473 K	O	4.6	2.65	0.013
	O	2.4	2.49	0.001
nano-CeO_{2-x}-623 K	O	5.5	2.30	0.027
nano-CeO_2-873 K	O	7.0	2.32	0.025
CeO_2	O	8.0	2.34	0.020

[a] *N*, *R*, and σ^2 refer to the coordination number, bond distances and Debye−Waller factors with respect to the first shell of Ce−O or Ce−N, respectively.

In the investigated system, the EXAFS of the as-prepared sample could not be fitted with the single Ce−O first shell as the standard CeO_2 but required two subshells at 2.64 and 2.47 Å, with the coordination numbers 6.3 and 6.2. When increasing the annealing temperature up to 473 K, the coordination numbers tend to be reduced and the bond length enhanced, indicating that the local structure has been more distorted. At annealing temperature above 623 K, the samples could be fitted with the single Ce−O first shell. Upon further increasing annealing temperature, both of the bond length and the coordination numbers are enhanced. Up to 873 K, the structural parameters listed in Table 2 are close to that for standard CeO_2. Therefore, when the annealing temperature is below 623 K, the structure feature of the sample is the transition from triclinic phase ($(CeNO_3)_3{\cdot}6H_2O$) to cubic phase (CeO_2). When the annealing temperature is above 623 K, the sample has similar features as that of the standard CeO_2, except the reduced coordination number and bond length, revealing that the nanocrystal CeO_2 is more distorted than that of standard CeO_2.

4. Discussion

As described in section 3, it is deduced that the as-prepared sample, obtained from cetyltrimethylammonium bromide (CTAB), butanol, and $Ce(NO_3)_3{\cdot}6H_2O$ in cyclohexane, is essentially Ce compound coated with CTAB. Because the content of the Ce compound is less than 3.0 wt % for the as-prepared sample, the XRD pattern is dominated by CTAB. Meanwhile, the XAS spectra show that the electronic property of Ce is consistent with that of $Ce(NO_3)_3{\cdot}6H_2O$ standard. After increasing the annealing temperature up to 623 K, the coated CTAB layers melt, decompose, and oxidize, as shown in the TG−DTA curve. In the XRD pattern, the peaks corresponding to CTAB are gradually weakened and finally disappear. In this process, the XANES spectra indicate that the valence state of Ce has a transition from +3 to +4 in the investigated system, which is induced by the oxidation of Ce compound.

For the sample annealed at 623 K, it is observed from TG−DTA that the decomposition and oxidation of the CTAB have finished, and Ce compound is completely exposed to the air atmosphere, which can enhance the oxidation of Ce compound. The HRTEM picture and XRD pattern show that the sample is amorphous. Moreover, the XAS spectroscopy indicates the coexistence of Ce^{3+} and Ce^{4+} in the CeO_{2-x} nanoparticles and the structural transformation of the sample from triclinic to cubic phase.

Upon further increasing the annealing temperature up to 773 K, the oxidation of the Ce compound is conducting sufficiently and CeO_2 nanocrystals form, as evidenced in the XRD patterns. As known,[20,26] many factors, such as the temperature and pressure, can influence the formation of nanocrystals. Essentially, all factors involve changeing the intrinsic energy and/or inherent stress, especially, which can be promoted by raising the annealing temperature. In this case, the structure of the system is changed by structural relaxation and reconstruction from a mestable or unstable structure to a stable one, as the intrinsic energy and/or inherent stress are large enough. In fact, it is observed from the XAS spectra that the valence state of cerium has completely changed from Ce^{3+} to Ce^{4+}, and its local structure has varied from triclinic to cubic when the annealing temperature is above 773 K.

(26) Zhang, H. Z.; Bandield, J. F. *J. Phys. Chem. B* **2000**, *104*, 3481.

The phenomena in our study are different from that of ref 15, in which there are no valence state transitions during the formation of CeO_2 nanocrystals. This is because the CeO_2 nanocrystals in ref 15 were prepared by precipitation of $Ce(SO_4)_2 \cdot 4H_2O$ with ammonia followed by an aging process. Therefore, the Ce valence remains +4 in the nanocrystalline CeO_2. However, in our work, as described in the Experimental Section, $Ce(NO_3)_3.6(H_2O)$ has been used as the precursor of CeO_2. With increasing calcination temperature, the Ce valence state changes from +3 to +4. These results mean that the formation mechanism of CeO_2 nanocrystals can be governed by the chemical nature of the precursor. Further effort is ongoing in our group to compare the structure and properties of CeO_2 nanocrystals derived from different precursors.

5. Conclusion

Microstructure development of cerium oxide nanocrystals, prepared by a microemulsion process, has been investigated as a function of the annealing temperature. At the beginning, the as-prepared sample is essentially Ce compound coated with CTAB, and its electronic property is similar to that of $Ce(NO_3)_3.6(H_2O)$. Between 298 and 623 K, the coated CTAB layers are gradually decomposed, finally exposing Ce compounds expose to the air atmosphere. At this moment, there is a coexistence of the +3 and +4 electronic states, and the local structure transitions from triclinic to cubic. Further increasing the temperature reconstructs the system structure. It is found that the phase structure changes from triclinic to cubic (CeO_2) and the corresponding valence state varies from Ce^{3+} to Ce^{4+}. Finally, the CeO_2 nanocrystals form when the annealing temperature is above 773 K.

Acknowledgment. The authors are indebted to Z. Z. Jie for her technical assistance in HRTEM photography.

CM010235P